Modern Health Science; Vol. 8, No. 3; 2025
ISSN 2576-7291 E-ISSN 2576-7305
https://doi.org/10.30560/mhs.v8n3p116

The Crystal Structures and Cytotoxicity of Two Copper(II) Complexes Synthesized in a Reaction System

Hongyu Lin[1,#], Yubin Mo[2,#] & Xiuying Qin[1]

[1] College of Pharmacy, Guilin Medical University, China

[2] Pharmacy Department, Guilin Women's and Children's Hospital, China

[#] These authors contributed equally to this paper.

Correspondence: Xiuying Qin, College of Pharmacy, Guilin Medical University, Guangxi, Guilin, 541004, China. E-mail: xyqin6688@163.com

Received: September 1, 2025; Accepted: September 16, 2025; Published: September 17, 2025

Abstract

Breast cancer poses a serious threat to women's health. In this study, we obtained two different copper-based complexes (I) and (II) in a reaction system, and characterized their crystal structures using X-ray single crystal diffraction technology. Additionally, the cytotoxic effects of these two copper complexes on two breast cancer cell lines (MCF-7 and MDA-MB-231) ,non-cancerous human umbilical vein endothelial cells (HUVECs) and normal human liver cells (LO2) were evaluated using the MTT assay. The obtained results provided certain theoretical and practical foundations for the development of potential anti-cancer drugs.

Keywords: Copper (II) complex, Crystal structure, Cytotoxicity, Breast cancer cells, Vascular endothelial cells

1. Introduction

Breast cancer is one of the most common and threatening malignant tumors among women worldwide, with persistently high incidence and mortality rates. Despite significant advancements in diagnostic techniques and treatment modalities (such as surgery, chemotherapy, radiotherapy, targeted therapy, and immunotherapy) in modern medicine, issues such as drug resistance, tumor recurrence, and metastasis remain severe, seriously affecting the quality of life and long-term prognosis of patients. Therefore, exploring novel therapeutic strategies and drugs to address the limitations of existing treatments has become an important direction in current breast cancer research.

In recent years, metal-based drugs have shown increasingly broad application prospects in cancer treatment. Since the advent of cisplatin (Cis-dichlorodiammine, platinum DDP) in the 1970s, it has greatly changed the treatment landscape of many cancers. Subsequently, second- and third-generation drugs such as carboplatin and oxaliplatin were developed, each with its own characteristics and widely used in clinical practice. Platinum-based metal drugs have broad-spectrum and highly efficient anti-tumor activity, with clear mechanisms of action and strong efficacy in killing cancer cells. However, platinum-based metal drugs also have some drawbacks during cancer treatment, mainly related to their side effects. For example, DDP has certain nephrotoxicity [1, 2], drug resistance [3, 4], and peripheral neurotoxicity [2]; carboplatin's main toxicity is myelosuppression (which may lead to a decrease in white blood cells, platelets, and red blood cells); oxaliplatin has certain acute neurotoxicity, manifested as abnormal sensations and even spasms in the throat, hands, and feet when exposed to cold, as well as chronic cumulative neuropathy. To reduce the toxic and side effects of drugs in the treatment of breast cancer, numerous studies on treatment regimens have emerged in recent years. For instance: targeted delivery systems, which encapsulate platinum drugs in liposomes to preferentially accumulate in tumor tissues and reduce damage to normal tissues; paclitaxel and carboplatin can assist in the treatment of triple-negative breast cancer [5]; antibody-drug conjugates (ADCs) can enhance the advantages of specific targeting and efficient killing to precisely and effectively eliminate cancer cells [6]. However, most of these approaches are relatively complex and costly. Therefore, developing an economical compound with good biological activity, low toxicity, and relatively simple structure for the treatment of breast cancer is of great significance.

Copper, as an essential trace element in the human body, plays a crucial role in various biological processes, including cellular energy metabolism, oxidative stress regulation, and signal transduction. Notably, copper ions and their complexes can exert anti-tumor effects through multiple mechanisms, such as inducing reactive oxygen

species (ROS) generation [7-9], promoting apoptosis [10], inhibiting angiogenesis [11-14], and interfering with tumor cell metabolism[15-22]. Compared with traditional platinum-based metal drugs, copper complexes may have lower toxicity and more unique mechanisms of action.

In this study, (I) and (II) were prepared by reacting L-tyrosine and 2,4-dihydroxy-3-methylbenzaldehyde as the main ligands with $Cu(NO_3)_2 \cdot 3H_2O$ in methanol solvent, and their crystal structures were obtained. The synthetic scheme is shown in Scheme 1. We investigated the structures and cytotoxicity of these two complexes, aiming to provide a reference for the screening of efficient, low-toxicity copper(II) complexes.

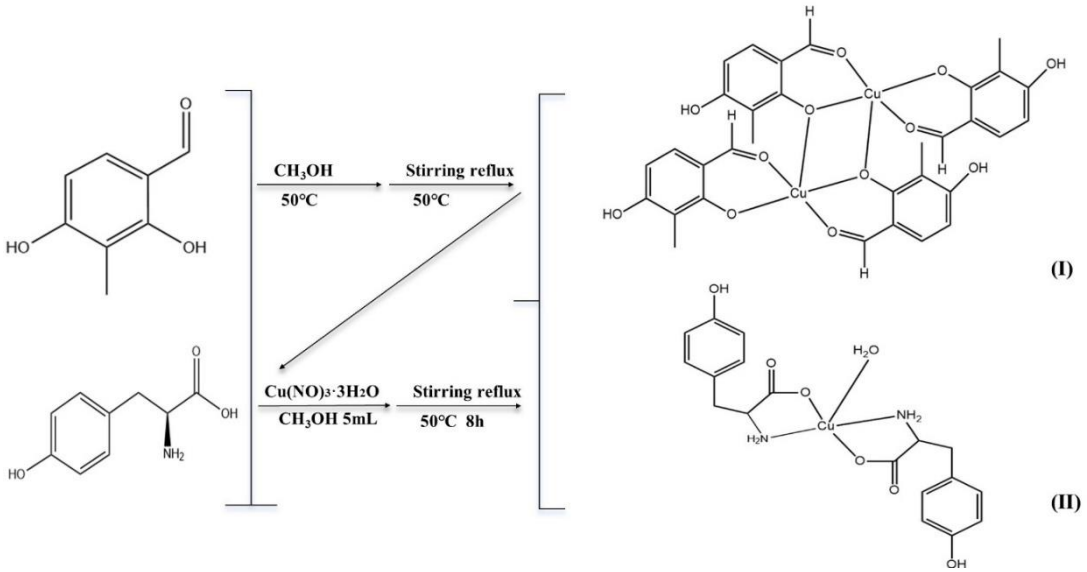

Scheme 1. Synthesis route of (I) and (II)

2. Materials and Methods

2.1 Experimental Reagents and Instruments

Materials. 2,4-Dihydroxy-3-methylbenzaldehyde (A.R.), L-tyrosine (A.R.), and copper(II) nitrate trihydrate (A.R.) were obtained from Aladdin. Anhydrous methanol (A.R.) was supplied by Xilong Technology Co., Ltd. Potassium hydroxide (R.G.) was purchased from Adamas. MTT, penicillin/streptomycin, dimethyl sulfoxide (DMSO), and bovine serum albumin (BSA) were acquired from Solarbio (Beijing, China). Dulbecco's Modified Eagle Medium (DMEM; Gibco), fetal bovine serum (FBS; GEMINI), trypsin (Gibco), and cell culture plates (Corning) were also used in this study.For cell culture, the complete medium was prepared by supplementing DMEM with 10% fetal bovine serum, 100 μg/mL penicillin, and 100 μg/mL streptomycin. Cells were maintained in a humidified incubator at 37°C under 5% CO_2 and 95% air atmosphere, with the medium refreshed every three days.

Instruments. Beaker, Round-bottom flask, Allihn condenser, Water bath. The crystal structures were determined by a four-circle CCD diffractometer (XtaLAB Synergy, Dualflex, HyPix).

2.2 Synthesis of (I) and (II)

A solution 1 was obtained by dissolving L-tyrosine (0.0362g, 0.2mmol) and potassium hydroxide (0.0337g, 0.6mmol) in an appropriate amount of anhydrous methanol; similarly, solution 2 was prepared by dissolving 2,4-dihydroxy-3-methylbenzaldehyde (0.0456g, 0.3mmol) in an appropriate amount of anhydrous methanol. Then, solution 2 was combined with solution 1 to obtain a mixed solution with a total volume of approximately 15 mL. The mixed solution was heated at a constant temperature of 50℃, stirred and refluxed for 2 hours, turning into a bright yellow solution, and the pH value of the solution was measured to be 7.2 - 7.5. $Cu(NO)_3.3H_2O$ (0.0751g, 0.3 mmol) was dissolved in 5 mL of anhydrous methanol, and then added to the aforementioned reaction system. The mixture was heated at a constant temperature of 50°C, stirred, and refluxed for 8 hours. The reaction mixture turned deep green and the pH was 6.4 - 6.7. After the reaction was completed, the naturally cooled reaction mixture was filtered to obtain a dark green filtrate. The filtrate was left to stand at room temperature and naturally evaporated. After several days, crystals were obtained. After several experiments, the crystal conditions obtained were as follows: (1) There were only dark yellow-green plate-like crystals (I) in the solution, as shown in Fig 1(C), and the maximum crystal yield was 26.56 mg; (2) There were both dark yellow-green plate-like crystals (I) (Fig

1(C)) and dark blue or dark blue-green needle-like or plate-like crystals (II) (as shown in Fig 2(B)), with the yield of (I) being approximately 6.12-10.56 mg and the yield of (II) being approximately 1.31-7.32 mg; (3) There were only very small amounts of dark blue-green plate-like crystals (II) in the solution, as shown in (d) in Fig 2(B), with a yield less than 1.0 mg. This may be affected by the occasional instability of the temperature controller, different reaction stirring speeds, the lack of deep purification of the reagents, and the slightly different crystal growth environment. The same experimental method and reagent dosage resulted in slight differences in the obtained crystals and their yields. However, the crystal morphology of the (I) crystals obtained in each experiment was almost the same, being yellow-green plate-like crystals, while the crystal color and morphology of the (II) crystals obtained in the experiments were slightly different, but the determined crystal structure was consistent. We randomly selected the crystals (I) and (II) synthesized from the same reaction system for the subsequent cytotoxicity study.

2.3 X-Ray Crystallography

Appropriate-sized single crystals (I) and (II) were selected respectively to determine the crystal structures. The crystallographic data of (I) and (II) were collected on a four-circle diffractometer (Type: XtaLAB Synergy, Dualflex, HyPix) equipped with X-ray mirror-monochromatized Cu K\a radiation (λ = 1.54184Å) in the omega scan mode at temperature 295.38(10) K. Using Olex2 1.5 application program.

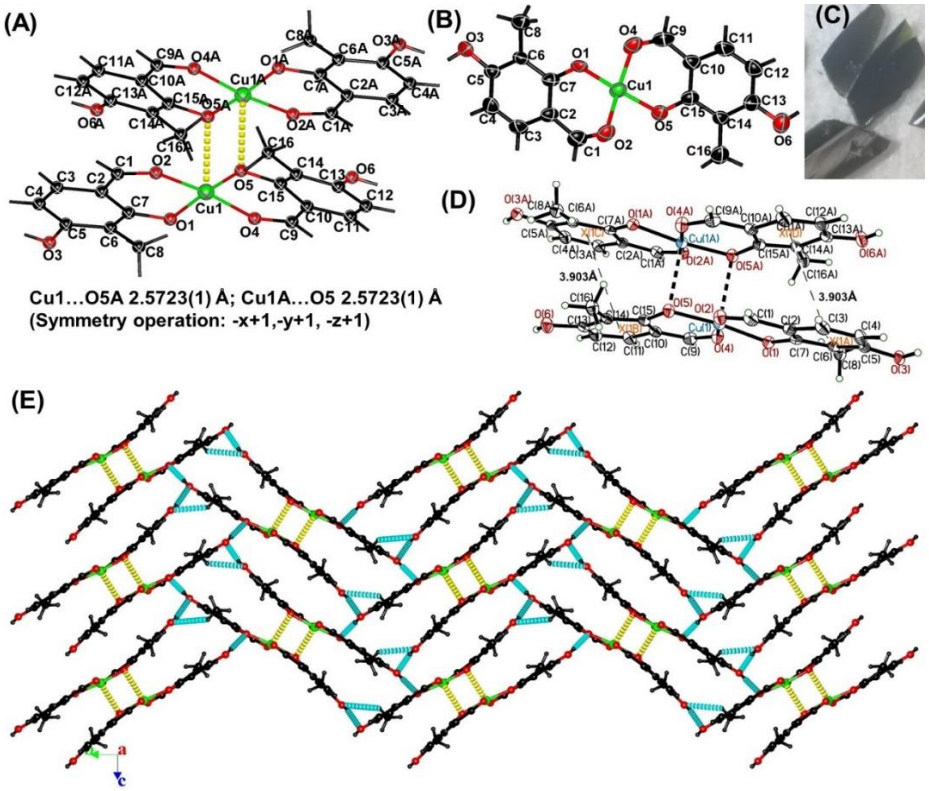

Figure 1. (A) Ellipsoidal structure diagram of half of (**I**) was drawn at the 50% probability level; (B) A complete ellipsoidal structure diagram of (**I**) was drawn at the 50% probability level, and the distance of the weak coordination bond between Cu1 and O5 is 2.5723(1) Å (Symmetry operation: -x+1, -y+1, -z+1); (C) The crystal morphology of (**I**), namely the dark yellow-green flaky crystals; (D) Through hydrogen bondings and π...π stackings, (**I**) stacks in the *bc* plane to form a two-dimensional network structure. In the figure, the light blue dotted lines represent hydrogen bonds, and the yellow dotted lines represent the weak coordination interaction between Cu1 and O5A and Cu1A and O5. For clarity, the π...π stacking effect has not been marked in the figure. [23], the .ins file of the crystal data was opened to solve the structure by the SHELXT 2018/2 (Sheldrick, 2018)program, and the crystal structure was refined using the SHELXL 2018/3 program[24]. All atoms were refined by anisotropic displacement parameters. All H atoms were calculated hydrogens, with C–H = 0.9300 Å for aldehyde group and aromatic [Uiso(H) = 1.2 Ueq(C)], with C–H = 0.9600 Å for methylene [Uiso(H) = 1.5 Ueq(C)], with C–H = 0.9700 Å for methylene [Uiso(H) = 1.2 Ueq(C)], with C–H = 0.9800 Å for sub-methylene [Uiso(H) = 1.2 Ueq(C)], with N–H = 0.8900 Å for amidogen [Uiso(H) = 1.2 Ueq(N)], with O–H = 0.8200 Å for hydroxyl [Uiso(H) = 1.5 Ueq(O)], and with O–H = 0.8505 Å for Coordination water molecule [Uiso(H) = 1.5 Ueq(O)].

2.4 Cytotoxicity Assay

The cell lines used in this study, including the breast cancer cell lines MCF-7 and MDA-MB-231 as well as the non-cancerous human umbilical vein endothelial cells (HUVECs), were obtained from.

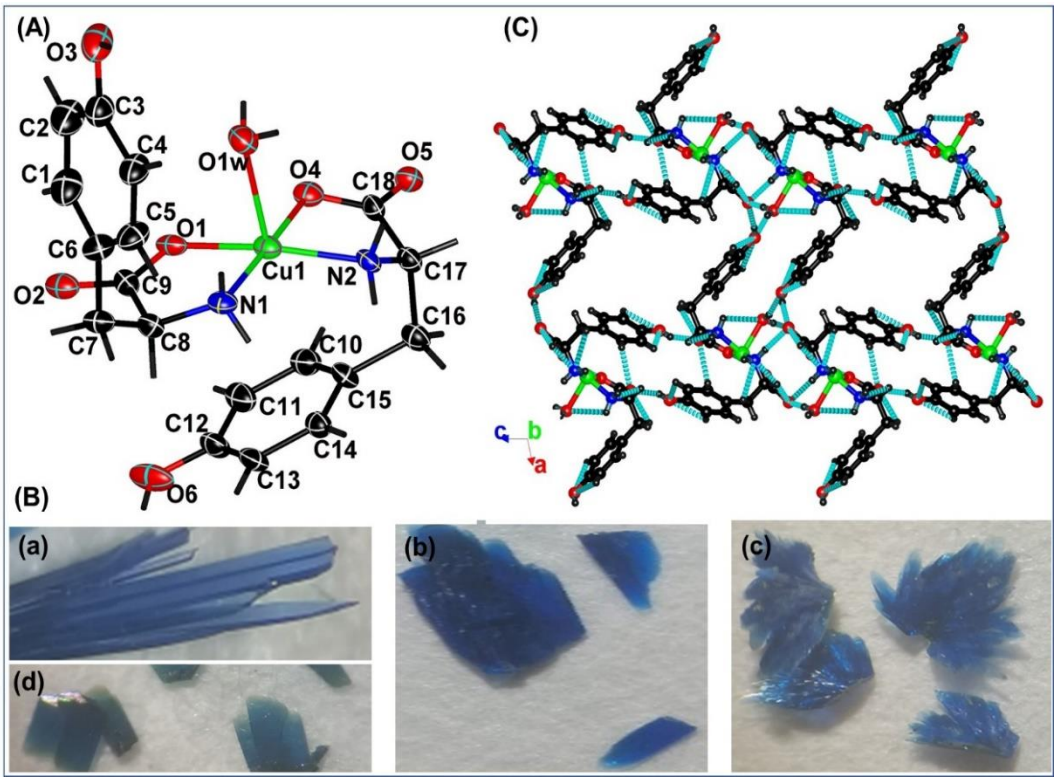

Figure 2. (A) The ellipsoidal structure diagram of (**II**) was drawn at the 50% probability level; (B) The crystal morphologies of (**II**), namely dark blue needle-shaped (a), dark blue sheet-like (b), and blue-green sheet-like (c,d) crystals; (C) Through hydrogen bondings, (**II**) stacks in the *ac* plane to form a two-dimensional layered network structure.

Shanghai Aolu Biotechnology Co., Ltd. All cells were cultured in high-glucose DMEM supplemented with 10% fetal bovine serum and 1% penicillin–streptomycin. All cells were cultured under standard conditions: 37°C, 5% CO_2, and 95% relative humidity in a humidified incubator. During the experiment, after 5000 cells were cultivated in each well for 24 hours, different concentrations of the metal complexes (I) and (II) were co-cultured with each cell line for 48 hours, respectively, and five replicates were set for each concentration. and then the MTT method was used to detect its cytotoxic effect. Then, the cytotoxicity was detected using the MTT method. The cell survival inhibition rate was calculated using the following formula:(Absorbance of control group − Absorbance of experimental group) / (Absorbance of control group − Absorbance of blank group) × 100%.The half-maximal inhibitory concentration (IC_{50}) was determined by nonlinear regression analysis using SPSS software.Additionally, GraphPad Prism was used for data visualization, including the generation of concentration-dependent inhibition bar charts, and for assessing statistical differences among the treatment groups.

Table 1. Crystal data and structure refinement parameters for (I) and (II).

Crystal parameters	(**I**)	(**II**)
Empirical formula	$C_{32}H_{28}Cu_2O_{12}$	$C_{34}H_{36}N_{10}NiO_5S_2$
Formula weight	731.62	441.91
Crystal system	Monoclinic	Monoclinic
a(Å)	7.8400(3)	11.8087(3)
b(Å)	23.4018 (9)	6.0153(2)
c(Å)	8.2438(4)	14.9179(4)
α(°)	90.00	90.00

β(°)	108.156(5)	101.832(2)
γ(°)	90.00	90.00
V(Å3)	1437.19(11)	1037.15(5)
Z	4	2
F(000)	748	458
M(mm-1)	2.433	1.847
Space group	P21/c	P21
Dc (g cm-3)	1.691	1.415
θ range(°)	6.2450-51.6040	5.3420-51.6660
Measured refls	2194	1845
Independent refls	1483	1772
Rint	0.0314	0.0315
Goodness	1.057	1.044
R1/wR2	0.0432/0.1235	0.0697/0.1842

Table 2. The selected bond distances (Å) for (I) and (II).

(I)					
Cu1-O1	1.899(3)	Cu1-O5	1.891(3)	Cu1-O2	1.961(3)
O1-C7	1.326(5)	O3-C5	1.356(5)	O5-C15	1.327(5)
O2-C1	1.256(5)	O4-C9	1.251(5)	O6-C13	1.363(5)
(II)					
Cu1-O1	1.938(9)	Cu1-O4	1.974(8)	Cu1-O1W	2.377(8)
Cu1-N2	1.987(10)	Cu1-N1	1.994(9)	O1-C9	1.265(15)
O4-C18	1.262(14)	O2-C9	1.266(16)	O5-C18	1.261(14)
N2-C17	1.475(13)	O6-C12	1.355(16)	N1-C8	1.466(14)
O3-C3	1.371(16)				

3. Results

3.1 The Crystal Structure of (I)

The crystallographic data indicate that the structure of (I) crystallizes in the monoclinic system, with the space group being P21/c. The main crystallographic parameters are as follows: a = 7.8400(3) Å, b = 23.4018(9)Å, c = 8.2438(4) Å, $\alpha = \gamma = 90°$, β = 108.156(5)°, V = 1437.19(11) Å3, Z = 2, Dc = 1.691 g/cm3, F (000) = 748, μ = 2.433 mm^{-1}, S = 1.057, $R1$= 0.0432, $\omega R2$ = 0.1235, Mr =731.62, Formula = $C_{32}H_{28}Cu_2O_{12}$. Other crystallographic data were presented in Table 1, coordination bond lengths and angles were shown in Table 2 and Table 3, and hydrogen bonds were depicted in Table 4. The crystal structure data have been deposited in the Cambridge Crystallographic Data Centre.(CCDC Number: 2484907; deposit@ccdc.cam.ac.uk). As shown in Figure 1(C), (I) presents a leaf-like, dark yellow-green crystal morphology. Figure 1(A) shows the crystal structure of (I), which consists of four second-hydroxyl-dehydrogenated 4-hydroxy-2-(hydroxyl)-3-methylbenzaldehyde ligands and two divalent copper ions, namely $[Cu_2(C_8H_7O_2)_4]$, bis[4-hydroxy-2-(hydroxyl)-3-methylbenzaldehydeato]-{μ-[4-hydroxy-2-(hydroxyl)-3-methylbenzaldehydeato]}-{μ-[4-hydroxy-2-(hydroxyl)-3-methylbenzaldehydeato]}-di-copper,
where H-($C_8H_7O_2$)= 2,4-dihydroxy-3-methylbenzaldehyde. Each pair of 4-hydroxy-2-(hydroxy)-3-methylbenzaldehyde ligands provides the dehydrogenation hydroxyl oxygen atoms (O1 and O5) and the oxygen atoms of the formaldehyde group (O2 and O4) to coordinate with a copper ion, forming a planar quadrilateral with five atoms (O1O2Cu1O4O5) almost coplanar, as shown in Figure 1(B). The bond lengths of these coordination bonds fall within the range of 1.891(3) to 1.961(3) Å (see: Table 2), which fall within the normal range of bond lengths for 4 or 5 coordination bonds; the angles of the coordination bonds < O1Cu1O2 = 92.37(12) °, < O1Cu1O4 = 86.26(11) °, < O5Cu1O2 = 87.17(12) °, < O5Cu1O4 = 93.37(12) °(see: Table 2), and the sum of these angles almost reaches 360°. Cu1 forms weak coordination bonds with O5A and Cu1A with O5, with a bond length of 2.5723(1) Å (symmetric operation: -x+1, -y+1, -z+1; see: Figure 1(A)), thus forming two five-coordinated tetragonal pyramid geometries for the entire coordination molecule. τ = (173.69-172.36)/60 = 0.022(see: Table 2), the value of τ being equal to 0 indicates that the five-coordinated coordination unit has a tetragonal pyramid geometry. Furthermore, there are π…π stacking effects in each coordination molecule, and the central distance between the benzene rings is 3.903 Å (X(1A)… X(1D), X(1B)… X(1C), Symmetry operation: -x+1, -y+1, -z+1), as shown in Figure 1(D). Typical hydrogen bondings (O-H...O, see: Table 3) and π...π stacking interactions

stabilize the structure of the entire molecule, causing (I) to stack in the bc plane and form a two-dimensional network structure, as shown in Figure 1(E).

Table 3. The selected bond angles (°) for (I) and (II)

			(**I**)		
O1-Cu1-O2	92.37(12)	O1-Cu1-O4	86.26(11)	O5-Cu1-O1	173.69(11)
O5-Cu1-O2	87.17(12)	O5-Cu1-O4	93.37(12)	O4-Cu1-O2	172.36(13)
C7-O1-Cu1	127.7(2)	C15-O5-Cu1	126.8(2)	C1-O2-Cu1	124.6(3)
C9-O4-Cu1	124.3(3)	O1-C7-C2	121.9(4)	O1-C7-C6	118.7(3)
O3-C5-C6	116.3(3)	O3-C5-C4	121.3(4)	O5-C15-C10	121.4(4)
O5-C15-C14	119.0(4)	O6-C13-C14	115.9(4)	O6-C13-C12	121.2(4)
O2-C1-C2	127.6(4)	O4-C9-C10	127.8(4)		
			(**II**)		
O1-Cu1-O4	94.5(3)	O1-Cu1-O1W	89.8(3)	O1-Cu1-N2	171.0(3)
O1-Cu1-N1	83.2(4)	O4-Cu1-O1W	95.4(3)	O4-Cu1-N2	82.9(4)
O4-Cu1-N1	177.4(4)	N2-Cu1-O1W	99.0(3)	N2-Cu1-N1	99.2(4)
N1-Cu1-O1W	85.7(4)	C9-O1-Cu1	116.0(8)	C18-O4-Cu1	113.4(7)
C17-N2-Cu1	106.8(7)	C8-N1-Cu1	111.2(7)	O1-C9-O2	121.8(11)
O1-C9-C8	118.6(11)	O2-C9-C8	119.5(11)	O4-C18-C17	118.1(10)
O5-C18-O4	123.2(11)	O5-C18-C17	118.7(11)	N2-C17-C18	108.1(9)
N2-C17-C16	111.1(9)	N1-C8-C9	108.7(9)	N1-C8-C7	112.9(9)
O6-C12-C13	122.5(12)	O6-C12-C11	117.6(13)		

Table 4. Hydrogen bond parameters for (I) and (II) (Å,°)

D-H···A	**D-H**	**H···A**	**D···A**	**D-H···A**
		(**I**)		
O3-H3···O1#1	0.82	1.86	2.774(13)	158.4
O6-H6···O3#2	0.82	1.97	2.763(4)	163.8
		(**II**)		
O1W-H1···WA#1	0.85	1.97	2.774(13)	158.4
O1W-H1···WB#2	0.85	2.00	2.805(14)	157.4
N2-H2A···O5#3	0.89	2.26	3.110(11)	160.8
O6-H6···O2#4	0.82	1.92	2.705(13)	158.9

Symmetry operation:

For Complex 1:(#1) – 0.5 + X, 1.5 – Y, – 0.5 + Z；(#2) 1.5 – X, – 0.5 + Y, 1.5 – Z.

For Complex 2:(#1)2 – X, 0.5 + Y,2 – Z；(#2) 1 – X, – 0.5 + Y,2 – Z；(#3) 1 – X, 0.5 + Y,2 – Z；(#4) 1 – X, 0.5 + Y,1 – Z.

3.2 The Crystal Structure of (II)

The crystallographic data suggest that the structure of (II) crystallizes in the monoclinic system, with the space group being P21. The main crystallographic parameters are as follows: a = 11.8087(3) Å, b = 6.0153(2)Å, c = 14.9179(4) Å, $\alpha = \gamma = 90°$, β = 101.832(2)°, V = 1037.15(5) Å3, Z = 2, Dc = 1.415 g/cm3, F (000) = 458, μ = 1.847 mm^{-1}, S = 1.044, $R1$ = 0.0697, $\omega R2$ = 0.1842, Mr = 441.91, Formula = $C_{18}H_{22}CuN_2O_7$. Other crystallographic data were presented in Table 1, coordination bond lengths and angles were shown in Table 2, and hydrogen bonds were depicted in Table 3. The crystal structure data have been deposited in the Cambridge Crystallographic Data Centre.(CCDC Number: 2484908; deposit@ccdc.cam.ac.uk). The crystal structure diagram of (II) is shown in Figure 2(A). The various crystal morphologies of (II) are shown in Figure 2(B). (II) is composed of two tyrosine anion ligands, one water molecule ligand and one divalent copper ion, namely [Cu $(H_2O)(C_9H_{10}N_1O_3)_2$], that is aqua-bis(tyrosinato)-copper, where H-$(C_9H_{10}N_1O_3)$= tyrosine. In the structure of (II), Cu1 is coordinated with two nitrogen atoms (N1 and N2) and two oxygen atoms (O1 and O4) from two tyrosine anion ligands and one oxygen atom (O1w) from molecule ligand to form a five-coordinated slightly deformed tetragonal pyramid geometry (τ = (177.4-171.0)/60 = 0.1067, the value of τ is only slightly greater than zero). In the tetragonal pyramid geometry,

the sum of the bond angles < O1Cu1O4 = 94.5(3) °, < O4Cu1N2 = 82.9(4) °, < N2Cu1N1 = 99.2(4) °, < N1Cu1O1 = 83.2(4) ° is 359.8° (see: Table 2), indicating that the copper ion (Cu1) is coplanar with the four coordinating atoms O1N1N2O4. O1w is the vertex of a tetragonal pyramid geometry. The bond length of coordination bond Cu- O1w (2.377(8) Å) is larger than those of coordination bond Cu-N and Cu-O, as shown in Table 2. The abundant hydrogen bonding interactions(O-H ... O and N-H ... O,) cause the (II) molecules to stack in ac plane, thereby forming a two-dimensional layered network structure(see Figure 2(C)). It is these intermolecular forces that stabilize the crystal structure of (II).

3.3 Cytotoxicity Analysis

To investigate the cytotoxicity of (I) and (II), we employed the MTT (3-(4,5-dimethylthiazol-2-yl)-2,5-diphenyltetrazolium bromide) method to determine the cytotoxicity of these two complexes against breast cancer cells (MCF-7), triple-negative breast cancer cells (MDA-MB-231), non-cancerous human umbilical vein endothelial cells (HUVECs), and normal human liver cells (LO2).

After co-incubation with MCF-7 cells for 48 hours, compared with the Control group, the cell density of MCF-7 cells significantly decreased as the concentration of (I) increased from 10.0 μM to 40.0 μM, and the cells became round and shrank, with some even undergoing lysis (see: Fig 3A); the survival inhibition rate of MCF-7 cells by (I) increased from (32.62 ± 0.92)% to (76.43 ± 0.17)% (see: Fig 4A), with a half-maximal inhibitory concentration (IC_{50}) of (11.58 ± 0.68) μM (see: Table 5). (I) exhibited a significant survival inhibition effect on MCF-7 cells. Under the same culture conditions, as the concentration of (II) increased from 40.0 μM to 160.0 μM, the density of MCF-7 cells also decreased (see: Fig 3A), and the inhibition rate increased from (32.84 ± 0.97)% to (62.42 ± 1.36)% (see: Fig 4B) (see: Fig 4A), indicating that high concentrations of (II) also inhibited the survival of MCF-7 cells, with an IC_{50} value of (69.72 ± 3.07) μM (Table 5). However, (I) had a higher cytotoxicity towards MCF-7 cells than (II).

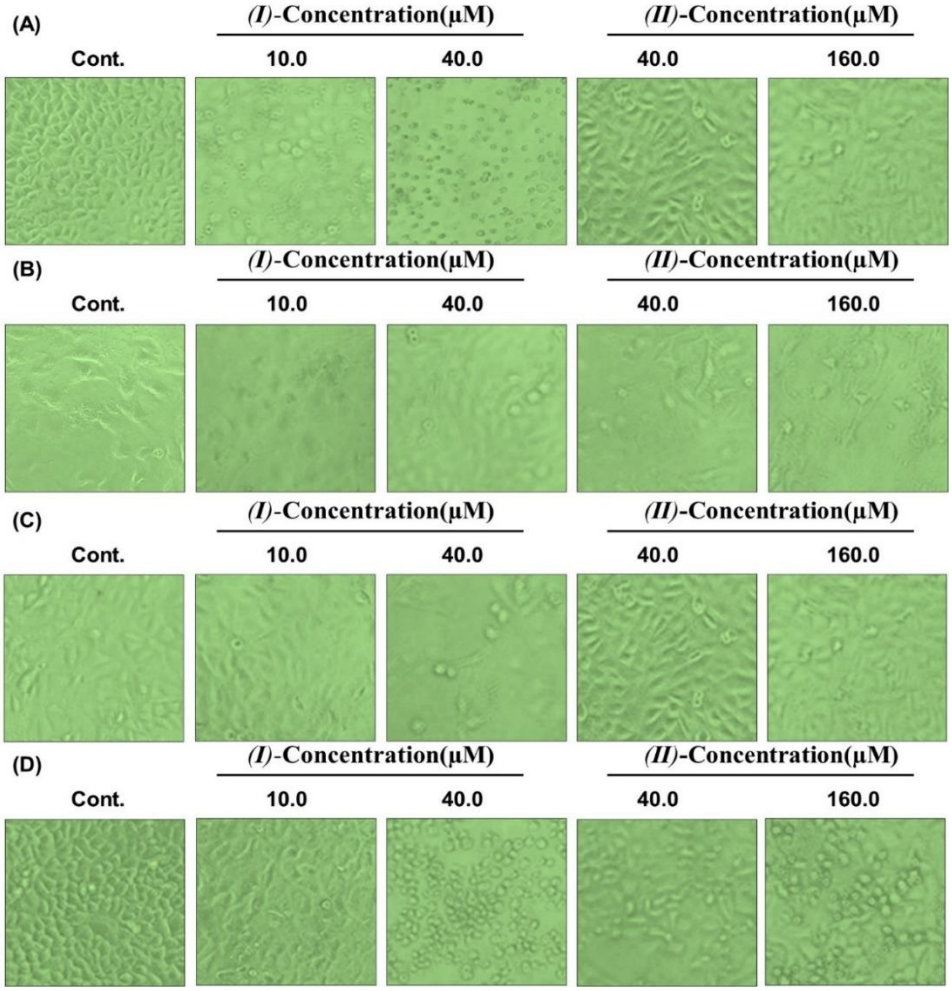

Figure 3. State diagrams of MCF-7 cells(A), MDA-MB-231 cells(B), HUVECs cells(C) and LO2 cells(D) under different sample concentrations

As shown in Fig 3B and Fig 4(A-B), in terms of cell density and survival inhibition rate, both (I) and (II) could slightly reduce the density of MDA-MB-231 cells. When the concentration of (I) increased from 10.0 μM to 40.0 μM, the survival inhibition rate of MDA-MB-231 cells increased from (10.38 ± 0.84)% to (51.85 ± 1.10)%, with an IC_{50} value of (47.78 ± 2.14) μM (table5); however, the IC_{50} value of (II) was >160 μM, as when the concentration of (II) reached 160.0 μM, the inhibition rate of MDA-MB-231 cells was only (29.14 ± 1.58)%.

HUVECs are often used to simulate the generation and inhibition of new blood vessels. Inhibiting the survival, proliferation, and migration of HUVECs can suppress the formation of tumor new blood vessels. As shown in Fig 3C and Fig 4(A-B), as the concentration of (I) gradually increased, compared with the Control group, the cell density decreased, and when the concentration reached 40.0 μM, the change in cell density was significant, with the survival inhibition rate of HUVECs increasing to (51.85 ± 1.10)%, and an IC_{50} value of 34.91 ± 2.48 μM (table5); however, (II) slightly inhibited the growth of HUVECs at concentrations between 20-80 μM, but when the concentration of (II) increased to 160 μM, the inhibition of HUVECs growth decreased instead. It is reported that copper is also a cofactor for angiogenesis, which may be because (II) is an amino acid copper complex and shows dual effects on non-cancerous HUVECs.

As shown in Figures 3D and 4(A-B), when (I) concentration was increased to 40.0 μM, the density of LO2 cells decreased, and the survival inhibition rate reached (89.66 ± 0.34)%, with an IC_{50} value of (14.13 ± 1.02) μM (Table 5); while when (II) concentration was raised from 40.0 μM to 160.0 μM, the cell density slightly decreased, and the cell survival inhibition rate increased to (28.18 ± 1.43)%, with an IC_{50} value > 160 μM.

The above results indicate that for the tested cells, (I) has higher cytotoxicity than (II), effectively inhibiting the growth of breast cancer cells, especially MCF-7 cells. (I) may also inhibit the survival and development of new blood vessel cells. This difference may be closely related to the choice of ligands and coordination modes of the complexes. Additionally, high concentrations of (I) also show significant cytotoxicity to normal LO2 cells, and thus should be used with caution.

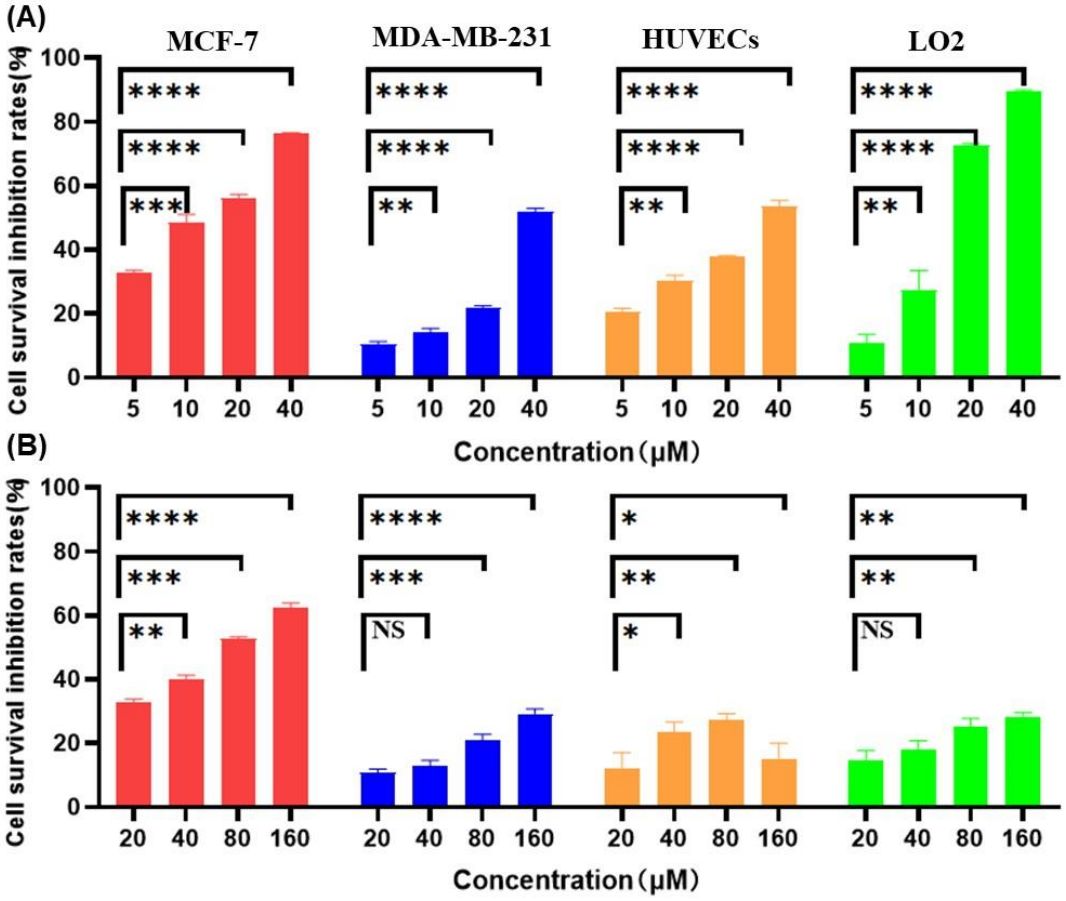

Figure 4. Explores the impact of different concentrations on the inhibitory rates of (I) and (II) against various cells. Statistical significance was determined between the treatment groups and the Control group for each cell type. * $p < 0.05$; ** $p < 0.01$; *** $p < 0.001$; **** $p < 0.0001$

Table 5. IC_{50}(μM) values of different cell lines treated with the experimental complexes for 48 h. Values are the mean ± SD of three independent experiments

	IC_{50}(μM)			
Complexes	**MCF-7**	**MDA-MB-231**	**HUVECs**	**LO2**
(**I**)	11.58 ± 0.68	47.78 ± 2.14	34.91 ± 2.48	14.13 ± 1.02
(**II**)	69.72 ± 3.07	>160[#1]	>160[#2]	>160[#3]

#1.When the concentration of (I) reached 160μM, the cells survival inhibition rate on MDA-MB-231 cells was (29.14 ± 1.58)%. #2.When the concentration of (I) reached 160μM, the cells survival inhibition rate on HUVECs cells was (15.20 ± 4.84)%. #3.When the concentration of (I) reached 160μM, the cells survival inhibition rate on LO2 cells was (28.18 ± 1.43)%.

4. Conclusions

In this study, using anhydrous methanol as the solvent, 2,4-dihydroxy-3-methylbenzaldehyde, potassium hydroxide, L-tyrosine, and copper(II) nitrate trihydrate were used as raw materials to obtain novel copper-based complexes (I) and (II) in a reaction system. The crystal structures of (I) and (II) were characterized by X-ray single crystal diffraction technology. The results showed that the crystals of (I) and (II) both belonged to the monoclinic crystal system, and the geometric structure of their coordination units was a tetragonal pyramid. The results of MTT analysis indicated that (I) had significantly higher cytotoxicity than (II). The IC_{50} value of (I) against MCF-7 cells was (11.58 ± 0.68) μM, against MDA-MB-231 cells was (47.78 ±2.14) μM, against HUVECs was (34.91± 2.48) μM, and against LO2 was (14.13± 1.02) μM demonstrating that (I) may inhibit the growth of breast cancer cells and the growth of new blood vessel endothelial cells. However, the IC_{50} value of (II) against MCF-7 cells was (69.72 ± 3.07) μM, and the survival inhibition rates of (II) against MDA-MB-231 cells, HUVECs cells and LO2 cells within the tested concentration range were relatively weak. The difference in cytotoxicity between (I) and (II) was due to the different ligands and coordination modes, reflecting the connection between the coordination complex structure and biological effect. This work provides certain insights for the future design of metal-based drugs.

References

[1] Loren, P., Lugones, Y., Saavedra, N., & Godoy, A. S. (2022). MicroRNAs involved in intrinsic apoptotic pathway during cisplatin-induced nephrotoxicity: Potential use of natural products against DDP-induced apoptosis. *Biomolecules, 12*(9), 1206. https://doi.org/10.3390/biom12091206

[2] Ma, X., Dang, C., Kang, H., & Chen, J. (2015). Saikosaponin-D reduces cisplatin-induced nephrotoxicity by repressing ROS-mediated activation of MAPK and NF-κB signalling pathways. *International Immunopharmacology, 28*(1), 399-408. https://doi.org/10.1016/j.intimp.2015.06.020

[3] Zhan, D., Ni, T., Wang, H., & Zhou, Z. (2022). Celastrol inhibits the proliferation and decreases drug resistance of cisplatin- resistant gastric cancer SGC7901/DDP cells. *Anti-Cancer Agents in Medicinal Chemistry, 22*(2), 270-279. https://doi.org/10.2174/1871520621666210528144006

[4] Yang, Z., Liu, Z., Ablise, M., & Yang, S. (2023). Design and synthesis of novel α-methylchalcone derivatives, anti-cervical cancer activity, and reversal of drug resistance in HeLa/DDP cells. *Molecules, 28*(23), 7697. https://doi.org/10.3390/molecules28237697

[5] Han, C., Liu, Z., Zhang, Y., Chen, J., Li, Y., Zhou, C., Wang, S., Zhang, S., Liu, M., Zhang, B., Xu, W., Chen, J., Wang, F., Shi, H., Wang, J., Yang, Y., & Dong, Y. (2020). Tumor cells suppress radiation-induced immunity by hijacking caspase 9 signaling. *Nature Immunology, 21*(5), 546-554. https://doi.org/10.1038/s41590-020-0641-5

[6] Liu, J., Liu, J., Guo, S. Y., Liu, C. M., & He, J. G. (2017). HSP70 inhibitor combined with cisplatin suppresses the cervical cancer proliferation in vitro and transplanted tumor growth: An experimental study. *Asian Pacific Journal of Tropical Medicine, 10*(2), 184-188. https://doi.org/10.1016/j.apjtm.2017.01.020

[7] Liu, H., Jiang, R., Lu, Y., Guo, Y., Zhang, W., Chen, X., Wang, Q., Liu, Q., Sun, Z., & Chen, X. (2022). Biodegradable amorphous copper iron tellurite promoting the utilization of Fenton-like ions for efficient synergistic cancer theranostics. *ACS Applied Materials & Interfaces, 14*(25), 28537-28547. https://doi.org/10.1021/acsami.2c03975

[8] Lomozová, Z., Hrubša, M., Conte, P. F., & Cvik, M. (2022). The effect of flavonoids on the reduction of cupric ions, the copper-driven Fenton reaction and copper-triggered haemolysis. *Food Chemistry, 394*, 133461.

https://doi.org/10.1016/j.foodchem.2022.133461

[9] Jomova, K., Cvik, M., Lauro, P., & Valentová, J. (2023). The role of redox active copper(II) on antioxidant properties of the flavonoid baicalein: DNA protection under Cu(II)-Fenton reaction and Cu(II)-ascorbate system conditions. *Journal of Inorganic Biochemistry, 245*, 112244. https://doi.org/10.1016/j.jinorgbio.2023.112244

[10] Jiang, Y., Huo, Z., Qi, X., Zhang, H., Cui, Y., & Yin, Y. (2022). Copper-induced tumor cell death mechanisms and antitumor theragnostic applications of copper complexes. *Nanomedicine, 17*(5), 303-324. https://doi.org/10.2217/nnm-2021-0374

[11] *Copper(II) complexes with 2,2':6',2"-terpyridine derivatives displaying dimeric dichloro-μ-bridged crystal structure: Biological activities from 2D and 3D tumor spheroids to in vivo models*. (n.d.). PubMed. Retrieved March 24, 2025, from https://pubmed.ncbi.nlm.nih.gov/36382103/

[12] Rodić, M. V., Leovac, V. M., Jovanović, L. S., Zmejkovski, B. B., & Vlahović, M. (2016). Synthesis, characterization, cytotoxicity and antiangiogenic activity of copper(II) complexes with 1-adamantoyl hydrazone bearing pyridine rings. *European Journal of Medicinal Chemistry, 115*, 75-81. https://doi.org/10.1016/j.ejmech.2016.03.003

[13] Draut, H., Rehm, T., Begemann, G., & Wiemann, T. (2017). Antiangiogenic and toxic effects of genistein, usnic acid, and their copper complexes in zebrafish embryos at different developmental stages. *Chemistry & Biodiversity, 14*(3). https://doi.org/10.1002/cbdv.201600302

[14] Zheng, H., Hu, C., Quan, Y., Song, C., Chen, S., Yu, X., Wang, Q., Zhang, X., & Liu, Q. (2023). A copper complex that combats triple negative breast cancer by restraining angiogenesis. *Dalton Transactions, 52*(22), 7626-7634. https://doi.org/10.1039/D3DT00738C

[15] da Silva, D. A., de Melo, A. C. C., Rodrigues, B. L., da Silva, A. M., de Oliveira, R. G. D., de Souza, B. G., Batista, A. A., & de Paula, E. (2022). Copper in tumors and the use of copper-based compounds in cancer treatment. *Journal of Inorganic Biochemistry, 226*, 111634. https://doi.org/10.1016/j.jinorgbio.2021.111634

[16] Liu, W. Q., Lin, W. R., Yan, L., Wu, D. B., Li, X. J., & Xu, J. (2024). Copper homeostasis and cuproptosis in cancer immunity and therapy. *Immunological Reviews, 321*(1), 211-227. https://doi.org/10.1111/imr.13276

[17] de Souza, Í. P., de Melo, A. C. C., Rodrigues, B. L., Santos, E. M. S., de Lima, M. E., de Castro, A. A. S., de Souza, B. G., & Batista, A. A. (2023). Antitumor copper(II) complexes with hydroxyanthraquinones and N,N-heterocyclic ligands. *Journal of Inorganic Biochemistry, 241*, 112121. https://doi.org/10.1016/j.jinorgbio.2023.112121

[18] Li, X., Chen, K., Lai, J., Lu, Z., Cao, Z., Yu, G., Li, S., Wang, H., & Liu, Y. (2024). Synthesis and antitumor activity of copper(II) complexes of imidazole derivatives. *Journal of Inorganic Biochemistry, 260*, 112690. https://doi.org/10.1016/j.jinorgbio.2024.112690

[19] Diz, M., Durán-Carril, M. L., Castro, J., & Bedia, J. C. (2022). Antitumor activity of copper(II) complexes with Schiff bases derived from N'-tosylbenzene-1,2-diamine. *Journal of Inorganic Biochemistry, 236*, 111975. https://doi.org/10.1016/j.jinorgbio.2022.111975

[20] Marzano, C., Pellei, M., Tisato, F., & Santini, C. (2009). Copper complexes as anticancer agents. *Anti-Cancer Agents in Medicinal Chemistry, 9*(2), 185-211. https://doi.org/10.2174/187152009787313837

[21] Miglioli, F., De Franco, M., Bartoli, J., Piacenza, L., Tosi, G., Gandin, V., & Marzano, C. (2024). Anticancer activity of new water-soluble sulfonated thiosemicarbazone copper(II) complexes targeting disulfide isomerase. *European Journal of Medicinal Chemistry, 276*, 116697. https://doi.org/10.1016/j.ejmech.2024.116697

[22] Jin, N., Zhang, L., & Qin, Y. X. (2025). Synthesis and crystal structure as well as cytotoxicity analysis of dichloro-terpyridine-copper complex. *Modern Health Science, 8*(2), 35-35. https://doi.org/10.30560/mhs.v8n2p35

[23] Dolomanov, O. V., Bourhis, L. J., Gildea, R. J., Howard, J. A. K., & Puschmann, H. (2009). OLEX2: A complete structure solution, refinement and analysis program. *Journal of Applied Crystallography, 42*(2), 339-341. https://doi.org/10.1107/S0021889808042726

[24] Sheldrick, G. M. (2015). Crystal structure refinement with SHELXL. *Acta Crystallographica Section C: Structural Chemistry, 71*(1), 3-8. https://doi.org/10.1107/S2053229614024218